Dalton Transactions

Accepted Manuscript

ROYAL SOCIETY OF CHEMISTRY

www.rsc.org/dalton

Figure 1. TEM images of (a and b) 10% CeO_2-g-C_3N_4, (c) HRTEM image of the CeO_2 cubes.

Figure 2. XRD pattern of g-C_3N_4 and the CeO_2/g-C_3N_4 composites.

Figure 3. C 1s (a), N 1s (b) and (c) O 1s XPS spectra, (d) High-resolution Ce 3d spectra.

Figure 4. (a) FT-IR spectra and (b) UV-visible absorption spectra of the g-C_3N_4 and CeO_2/g-C_3N_4, (c) estimated band gaps of the g-C_3N_4 and CeO_2/g-C_3N_4, (d) photocurrent-time dependence of the g-C_3N_4 and 2.5%, 5%, 10% CeO_2/g-C_3N_4 electrodes in $NaNO_3$ (0.1 M) aqueous solution under visible light irradiation.

Figure 5. (a) The photocatalytic degradation of MB dye by the photocatalysts, (b) the kinetics of MB degradation using various photocatalysts under visible-light irradiation, (c) cycling runs for the photocatalytic degradation of MB in the presence of 5% CeO_2/g-C_3N_4 under visible light irradiation.

Figure 6. (a) XRD patterns and (b) FT-IR spectra of 5% CeO_2/g-C_3N_4 before and after the cycling photocatalytic experiments.

Figure 7. (a), (b), (c) and (d) changes in UV-visible absorption spectra of MB by g-C_3N_4 and CeO_2/g-C_3N_4 composites.

Figure 8. (a) Photocurrent intensity of ITO/5% CeO_2/g-C_3N_4 in the presence of different Cu^{2+} concentrations, (b) plot of photocurrent I of ITO/5% CeO_2/g-C_3N_4 versus Cu^{2+} concentration, (c) photocurrent intensity of ITO/5% CeO_2/g-C_3N_4 in the presence of 4.0 μM solutions of various metal ions.

Figure 9. Schematic illustration of exciton trapping mechanism and photoelectrochemistry for sensing of trace amounts of Cu^{2+}.

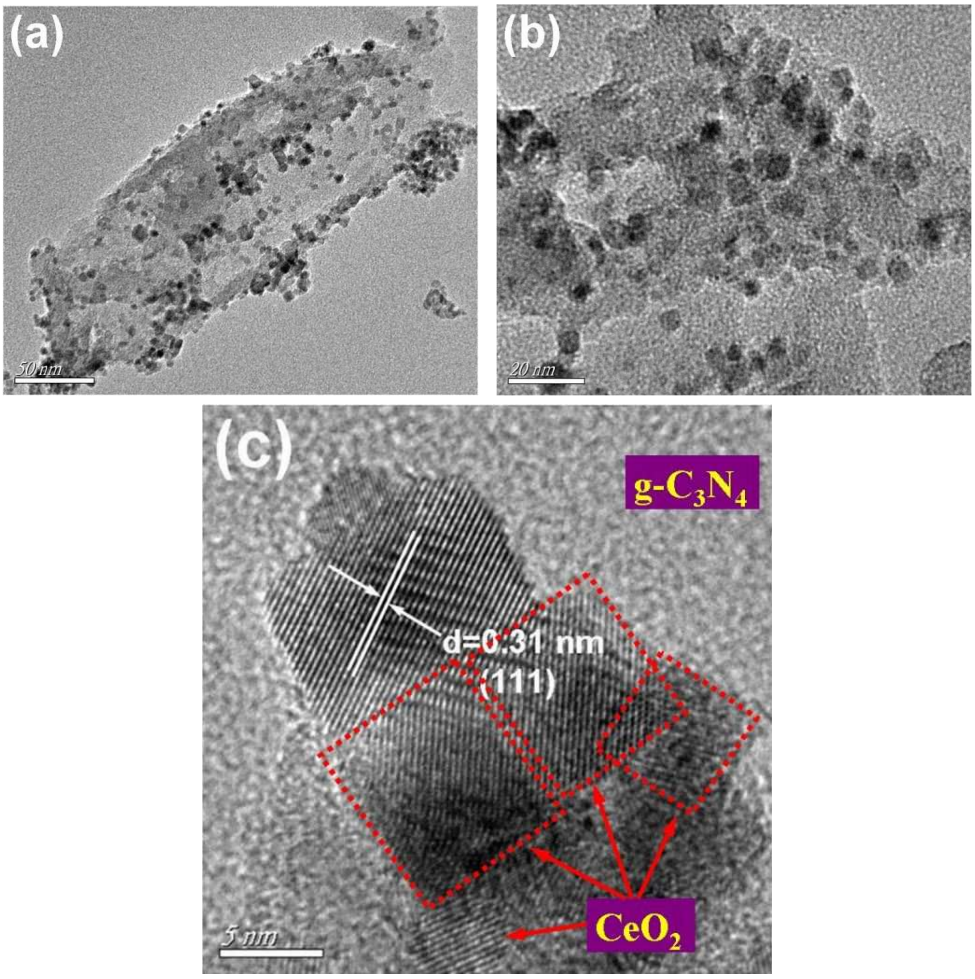

Figure 1

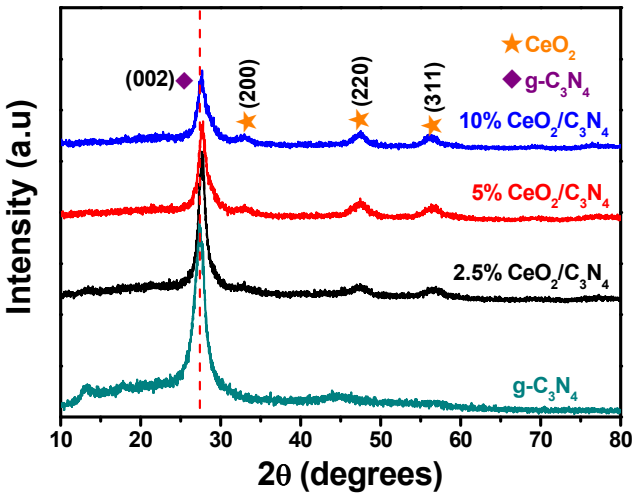

Figure 2

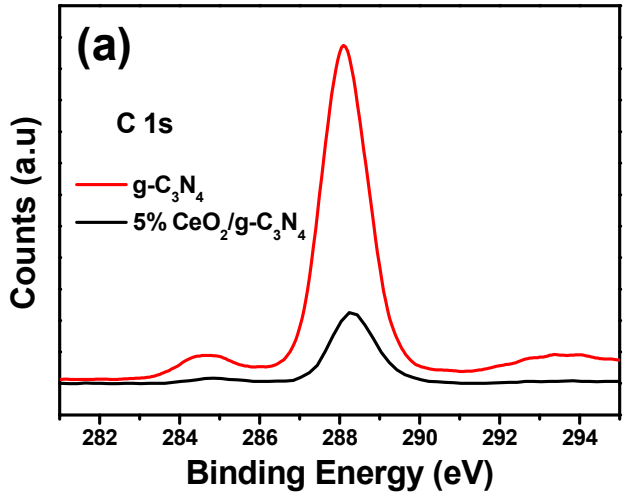

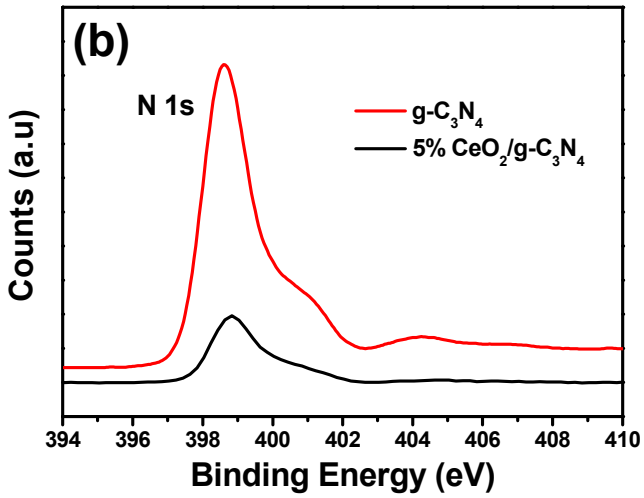

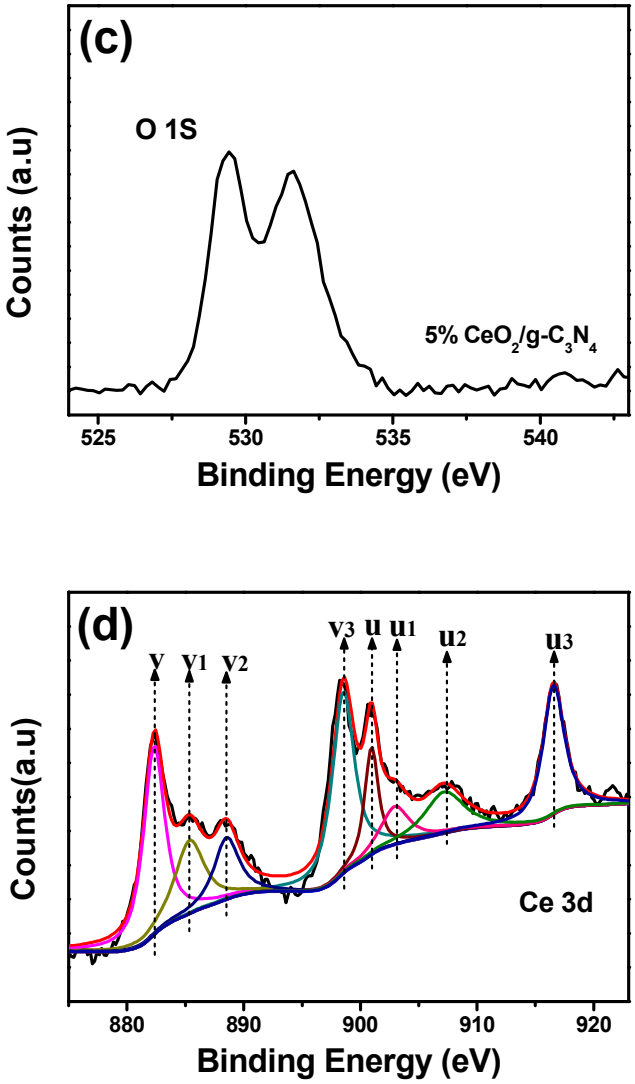

Figure 3

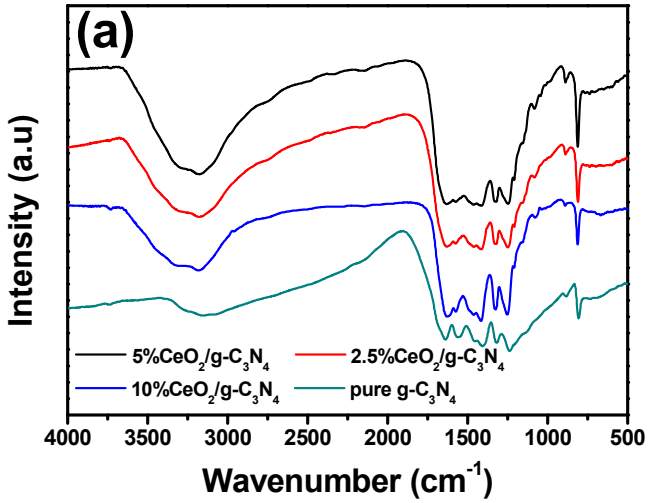

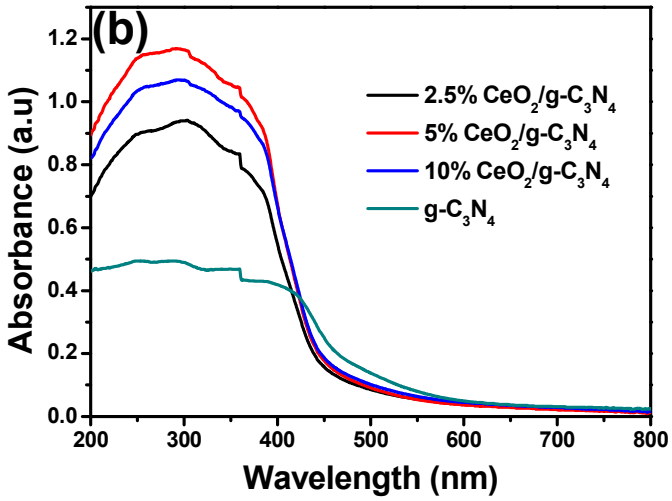

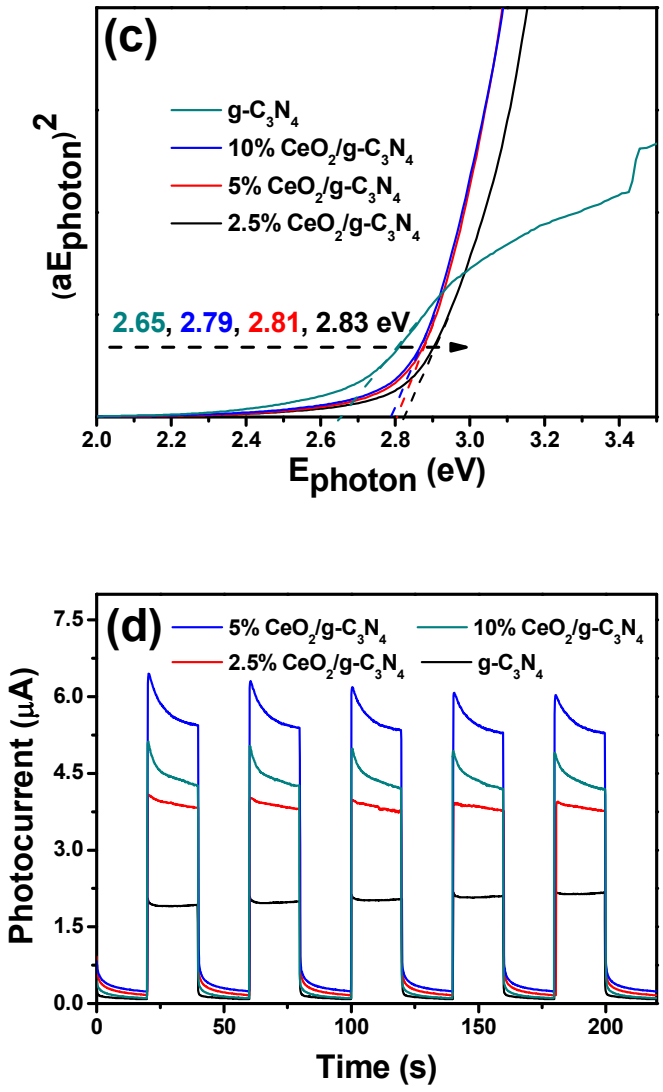

Figure 4

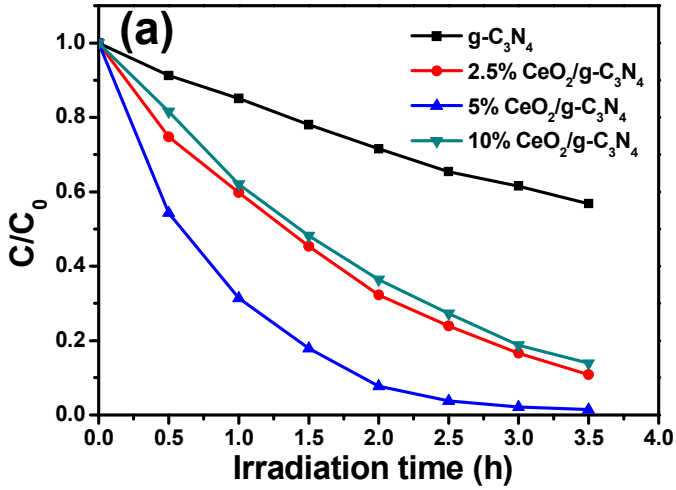

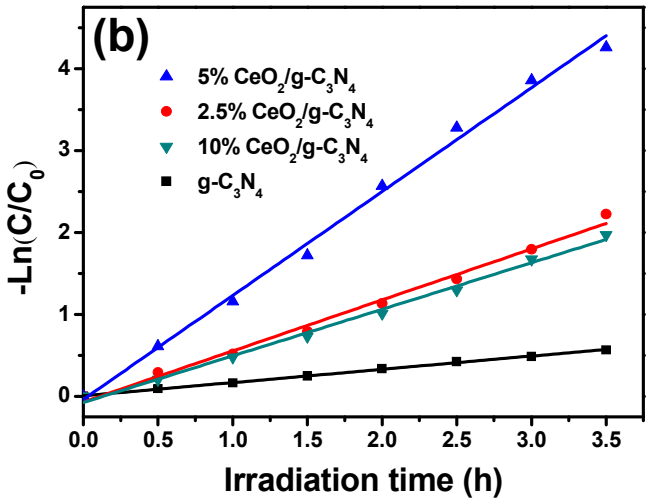

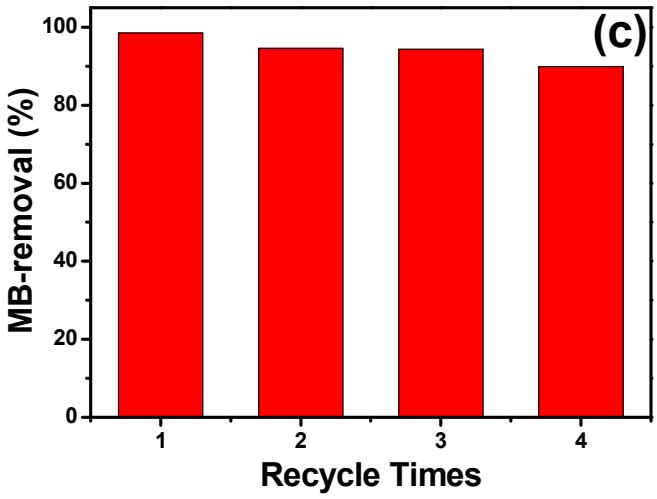

Figure 5

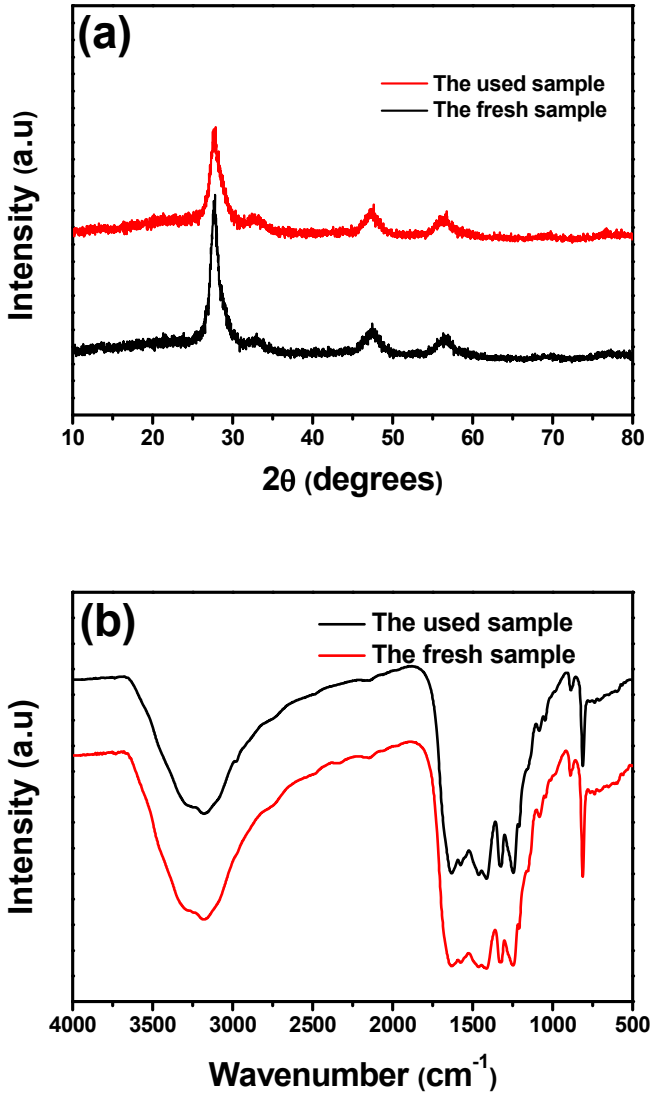

Figure 6

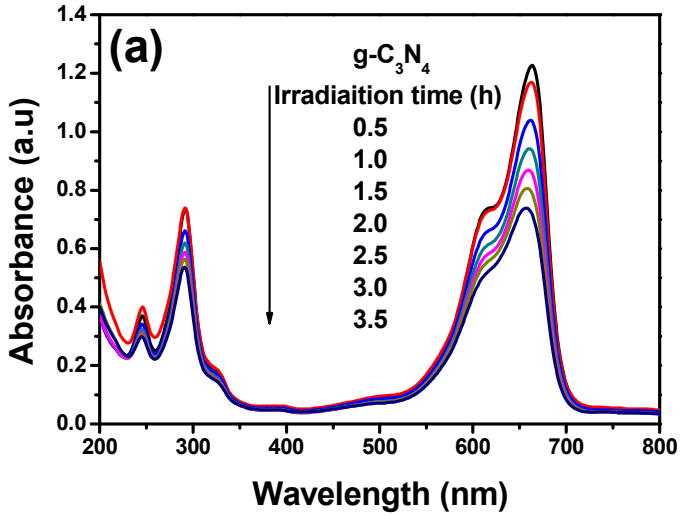

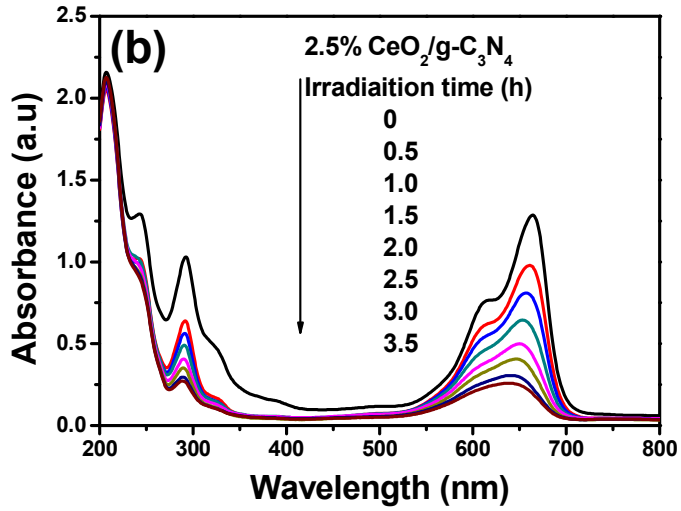

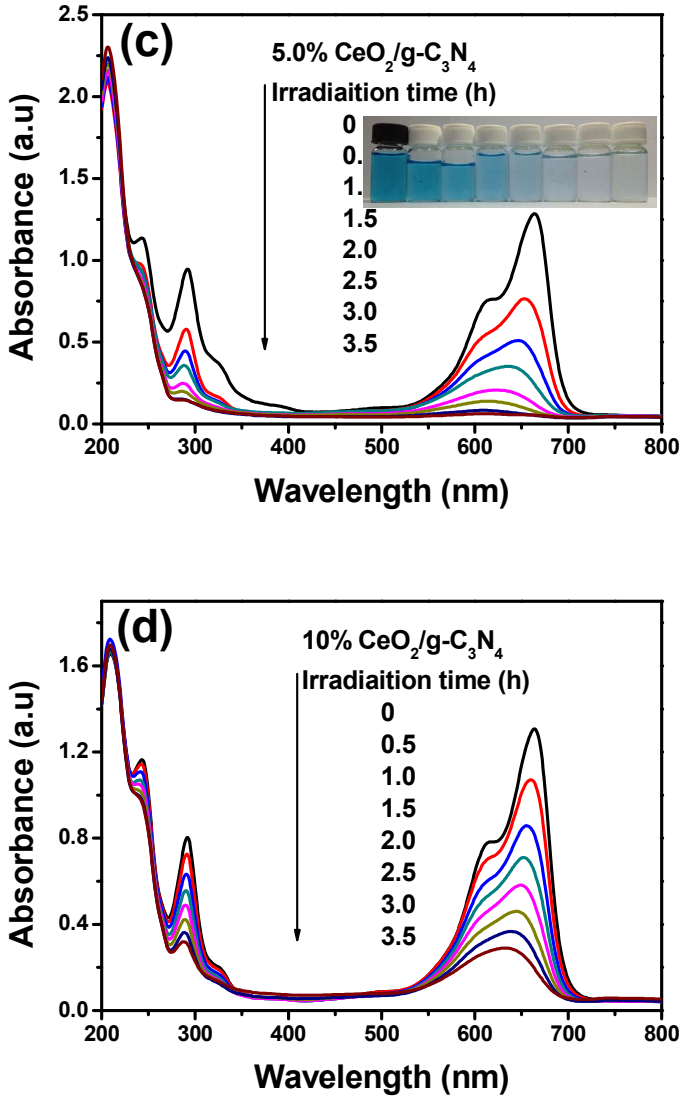

Figure 7

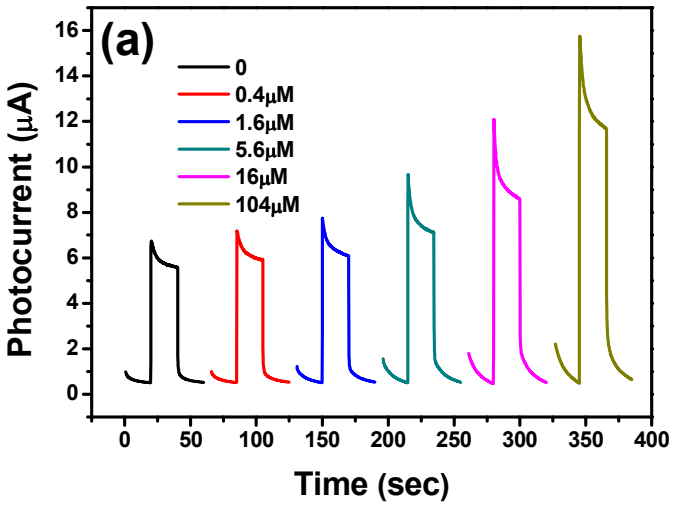

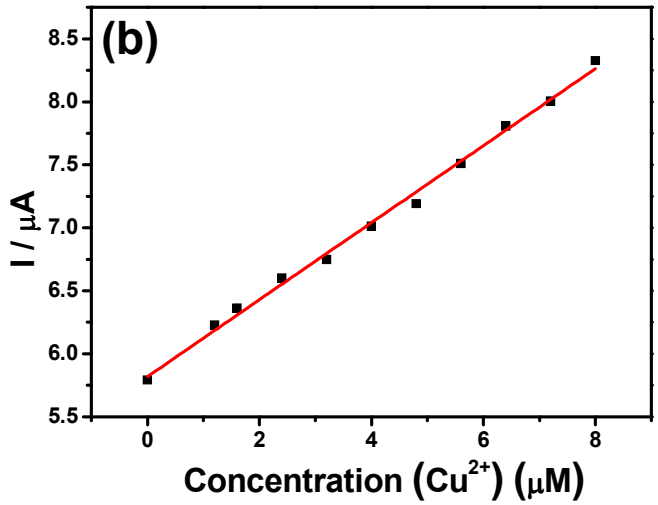

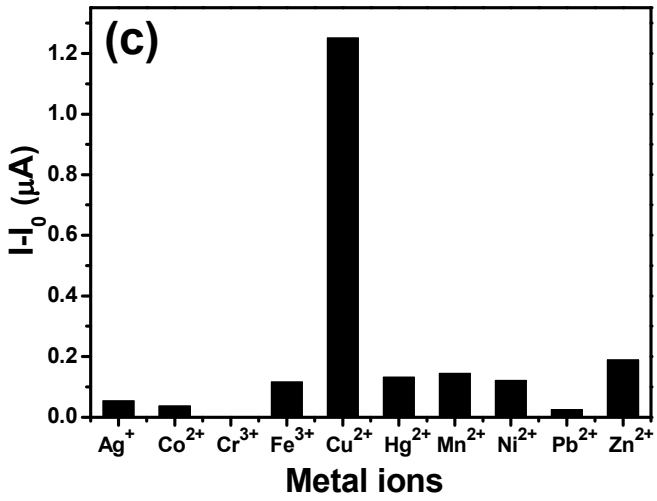

Figure 8

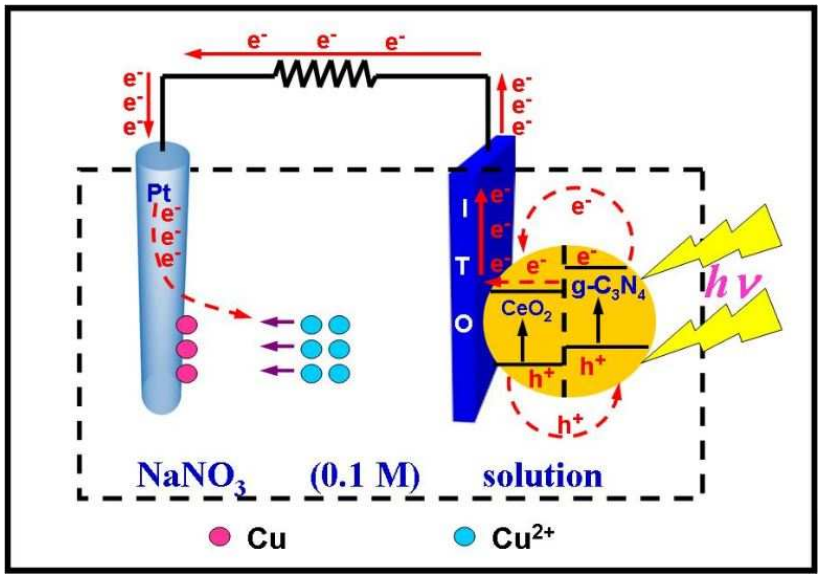

Figure 9

Table 1. Kinetic Constants and Regression Coefficients of MB Degradation under Visible Light Irradiation.

Table 1.

Photocatalysts	Kinetic constant (k, h^{-1})	R^2
g-C_3N_4	0.1621	0.9984
2.5% CeO_2/g-C_3N_4	0.6226	0.9908
5% CeO_2/g-C_3N_4	1.2686	0.9944
10% CeO_2/g-C_3N_4	0.5687	0.9939

Controllable synthesis of CeO_2/g-C_3N_4 composites and their applications in environment

Xiaojie She, Hui Xu,* Hefei Wang, Jiexiang Xia, Yanhua Song, Jia Yan, Yuanguo Xu, Qi Zhang, Daolin Du, and Huaming Li*

School of the Environment, Institute for Energy Research, Jiangsu University, Zhenjiang 212013, P. R. China

***Corresponding author:** Tel.:+86-511-88791800; Fax: +86-511-88791708;
E-mail address: xh@ujs.edu.cn, lihm@ujs.edu.cn

Through the hydrothermal method, the ultrafine CeO_2 cubes and g-C_3N_4 formed the heterojunction structure. And the homogeneous dispersedness of CeO_2 cubes on g-C_3N_4, effective combination of ultrafine CeO_2 cubes on g-C_3N_4 and high crystallinity of CeO_2 improved the photocatalytic activity of CeO_2/g-C_3N_4 nanocomposites. Meanwhile, 5% CeO_2/g-C_3N_4 gave other birth to new promising properties: highly selective and sensitive sensor for the detection of trace amount of Cu^{2+}. And the exploited novel photocatalytic reactor insured the efficiency of photocatalytic reaction.

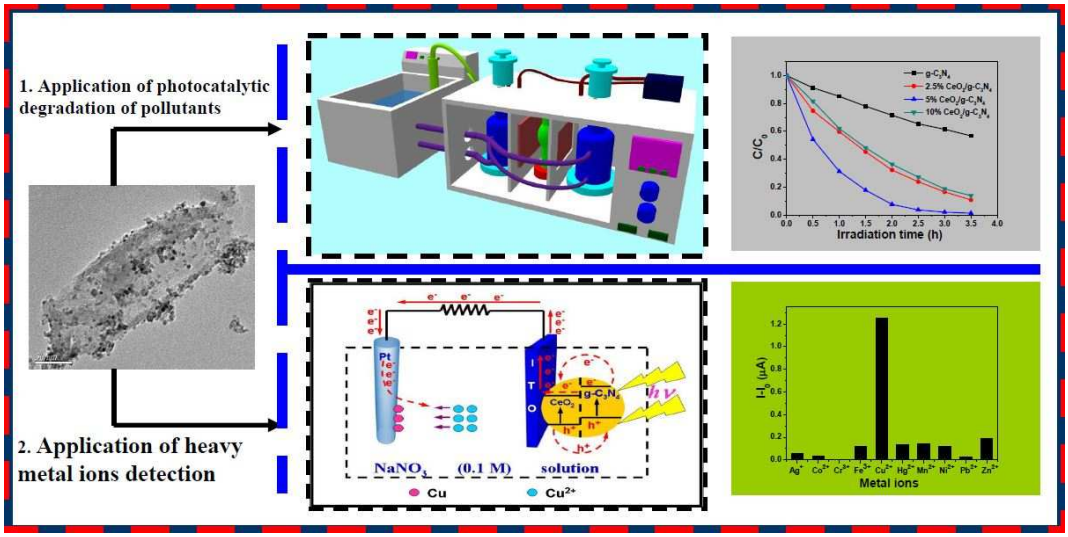

Controllable synthesis of CeO_2/g-C_3N_4 composites and their applications in environment

Xiaojie She, Hui Xu,* Hefei Wang, Jiexiang Xia, Yanhua Song, Jia Yan, Yuanguo Xu, Qi Zhang, Daolin Du, and Huaming Li*

School of the Environment, Institute for Energy Research, Jiangsu University, Zhenjiang 212013, P. R. China

***Corresponding author:** Tel.:+86-511-88791800; Fax: +86-511-88791708;

E-mail address: xh@ujs.edu.cn, lihm@ujs.edu.cn

ABSTRACT:

The experiment developed a photocatalytic reactor which includes circulating water, light, and temperature control system. CeO_2/g-C_3N_4 composites with high photocatalytic activity and stability were synthesized by a simple and facile hydrothermal method. The obtained photocatalysts were characterized by X-ray diffraction (XRD), transmission electron microscopy (TEM) and X-ray photoelectron spectroscopy (XPS). It is found that in CeO_2/g-C_3N_4 composites, CeO_2 presented homogeneous shape of the cube (from 3 to 10 nm) and it was equably dispersed on the surface of g-C_3N_4. At constant temperature (30°C), 5% CeO_2/g-C_3N_4 photocatalyst showed the best photocatalytic activity for degrading organic dye methylene blue (MB) under visible light irradiation. And the photocatalytic reaction for MB followed first-order kinetics and 5% CeO_2/g-C_3N_4 exhibited a higher apparent rate of 1.2686 min^{-1}, which was 7.8 times as high as that of the pure g-C_3N_4 (0.1621 min^{-1}). What's more, it was found that 5% CeO_2/g-C_3N_4 had a new property that it could be used as the sensor for tracing amounts of Cu^{2+} determination. Such unique design and one-step synthesis with an exposed high-activity surface are important for both technical applications and theoretical investigations. Moreover, the excellent photocatalytic reactors were exploited, so it could promote further development of photocatalysis technology.

1 Introduction

In order to further solve the energy dilemma, the problems of environmental pollution and enhance the application of solar energy, photocatalysis has become one of the most promising technology, both in field of research and in industrial applications. The ideal photocatalyst should be activated as well as stable for decreasing the economic and environmental costs of potential metallic or toxic elements' secondary pollution. However, both high-powered photocatalyst and excellent photocatalytic reactors limited the development of the photocatalysis technology. Typically, due to large bandgap,[1,2] the excellent and stable metal oxide photocatalyst TiO_2 has no or limited visible light absorption, which does not meet the requirements for the industry. So, in order to solve these problems, the researchers has taken many measures as changing the morphology of TiO_2,[3] loading of nonmetal,[4] constructing a heterojunction composite with another semiconductor[5] and dye sensitization.[6] Although, these approaches have resulted in some improvements of their photocatalytic performance, it still has not meet the requirements of industrial application. For the composites of TiO_2, the size of TiO_2 was unhomogeneous and quite large, the morphology of TiO_2 could not be controlled well and TiO_2 could not bond with another semiconductor. The composites were very unstable and showed low photocatalytic activity as a result. What's more, very few photocatalytic reactors can provide stable dynamic response environments. General photocatalytic reactors have some general problems. For example, light source is not stable because the bulb providing high intensity of visible light was usually broken, temperature control system was not satisfying because of some design defects, water circulation systems consumed energy, circuit security system could not ensure absolute safety and so on. For those reasons, the development of an efficient photocatalyst under visible-light and excellent reactors (or equipments) are still desired.

The graphitic carbon nitride (g-C_3N_4) that is the organic polymeric semiconductor material and is like the graphite owning layer structure, has attracted more and more attention from researchers, relying on its visible light response, high thermal and chemical stability, and abundant yet low-cost nitrogen-rich precursor materials.[7] As a

metal-free, nontoxic and organic semiconductor, g-C_3N_4 is made up of carbon and nitrogen. It shows great advantages in photocatalytic water splitting, photodegradation of environmental organic pollutants, electrochemical sensors and bioimaging,[8-10] so it becomes one of the most prospective photocatalyst. However, as photocatalyst, g-C_3N_4 also has some inevitable shortcomings, such as: high recombination rate of photoexcited charge carriers, low quantum efficiency, lower specific surface area, lack of absorption above 460 nm, the lesser active sites,[9,11,12] etc, which leads to low photocatalytic activity. With those disadvantages, the development of g-C_3N_4 is hampered badly. In order to solve these defects, many methods have been taken to improve the photocatalytic activity of g-C_3N_4 under visible light irradiation, such as chemical doping with foreign elements, preparing novel nanostructures, constructing a heterojunction composite with another semiconductor, etc. (Ag/g-C_3N_4,[13] AgX/g-C_3N_4,[9] ZnO/g-C_3N_4,[14] g-C_3N_4-WO_3,[15] C-60/g-C_3N_4,[16] and Cu_2O/g-C_3N_4[17]) Specially, the metal or metallic oxide-containing g-C_3N_4 composites (Fe/g-C_3N_4,[18] Co_3O_4/g-C_3N_4,[19] Fe_3O_4/g-C_3N_4,[20] TiO_2/g-C_3N_4,[21,22]) have been proved to be an effective photochemical oxidation catalysts under visible light irradiation. Obviously, the modification of g-C_3N_4 is very efficient as improving the optical absorption and photocatalytic performance under visible light irradiation. However, in the modification of g-C_3N_4 system, the light harvesting ability and quantum efficiency of the materials are still unsatisfying. Thus, it is still necessary to find an appropriate composites to further enhance the photocatalytic performance of g-C_3N_4 so that g-C_3N_4 can be exploited and applied in environment and industrial manufacture better.

CeO_2 has been reported as an efficient photocatalyst with a band gap (Eg = 2.92 eV), it absorbs light near UV and slightly in the visible light region,[23] CeO_2 is also one of the most important rare earth materials and it has been extensively studied for many technological applications including fuel cells, catalytic, luminescent and solar cells due to its chemical stability and high oxygen storage capacity.[24-27] What's more, many composites of CeO_2 have been prepared. Therefore, if CeO_2/g-C_3N_4 composite material could be obtained, it might be an excellent photocatalyst with visible-light

response. However, how to obtain high-powered, stable and homogeneous CeO_2 in composite material remains to be an intractable problem. Although, the various microstructures of CeO_2 and composites of CeO_2 (including CeO_2/Graphene,[24] and ultrathin mesoporous single-crystal-like CeO_2,[28]) have been prepared, in the synthesis of composite materials of CeO_2, getting a uniform, homogeneous size and a good morphology of CeO_2 with excellent performance was still very challanging. Because, firstly, the size of CeO_2 was very difficult to control; secondly, in many composites, whether CeO_2 could bond with other materials well and dispersed well were still the inevitable questions; thirdly, the ideal CeO_2's crystallinity was difficult to be obtained; fourthly, the dispersibility of CeO_2 in composite materials still perplexed the researchers, which leads to the result that the prepared composite materials of CeO_2 were not stable, even CeO_2 could drop from the composite material, when composite material was sonicated. Not to mention, the poor photocatalytic activity was also followed. Thus, how to control the size, morphology, binding force and dispersibility of CeO_2 in composite materials, is considered to be very significant. If CeO_2 in composite materials could be controlled and synthesized well, it is likely that the composite materials might have some exciting performances or applied further for environment or industrial manufacture. Extravagant hopes could also be possessed: if CeO_2/g-C_3N_4 composites were successfully prepared, and the homogeneous CeO_2 nanocubes could be dispersed well onto g-C_3N_4, and formed a heterojunction structure, it was hopeful that CeO_2/g-C_3N_4 composites may become a multi-function photocatalyst.

Within this work, we demonstrated the preparation of g-C_3N_4 and CeO_2/g-C_3N_4 composites, and investigated the effect of different mass ratios of CeO_2/g-C_3N_4 and the pure g-C_3N_4 on photocatalytic performance. Photocatalytic experiments for improving the accuracy of the experimental data, exploiting stable, controllable and high-efficiency photocatalytic reactor has also been performed. The model of the photocatalytic reactor and all parameters were revealed. Moreover, a novel feature was found that 5% CeO_2/g-C_3N_4 could be used for highly efficient photoelectrochemical selective sensing of trace amounts of Cu^{2+}, because of its higher

photocurrent intensity, compared with g-C_3N_4. In conclusion, CeO_2/g-C_3N_4 composite is a novel and promising candidate for heavy metal ions (Cu^{2+}) determination in water environment, which will promote the further development of photocatalytic materials in practical applications of the environment. The developed photocatalytic reactor could also support the light-catalyzed reaction well, which also may be the photocatalytic reactors for further development.

2. Experimental section

2.1 Preparation of the g-C_3N_4

As shown in **Figure S1**，the preparation of g-C_3N_4 was by heating dicyandiamide in the pipe furnace directly, 2g dicyandiamide was put into a crucible with a cover. Hit the temperature to 350°C within 90 min and kept 350°C for 2 h, and then made it rise to 600°C within another 90 min and kept 600°C for another 2 h. For consideration, the whole process of the reaction was taken under flowing-nitrogen atmosphere (200 ml/min). And the nubbly g-C_3N_4 was grinded into the powder before further characterizations, as shown in **Figure S1**.

2.2 Preparation of the CeO_2/g-C_3N_4

The g-C_3N_4 (0.1 g) and a certain quantity of $Ce(NO_3)_3 \cdot 6H_2O$ were added into 19 mL of H_2O, and the suspension was stirred magnetically for 30 min, and then was sonicated for 30 min. Subsequently, 0.5 mL of $NH_3 \cdot H_2O$ was injected into the mixture under magnetic stirring. Then, the mixture was transferred into a Teflon-lined stainless steel autoclave with 20 mL of capacity and the sealed tank was put into an oven and heated at 160°C for 12 h. The resulting product was separated by centrifuging and washed several times with distilled water and ethanol, respectively. Finally, the obtained composites were dried in air at 60°C for 8 h. According to this method, different molar ratios of the CeO_2/g-C_3N_4 samples were obtained and denoted as 2.5% CeO_2/g-C_3N_4, 5% CeO_2/g-C_3N_4 and 10% CeO_2/g-C_3N_4.

2.3 Photoelectrochemical measurements

The photocurrents were measured with an electrochemical analyzer (CHI660B, Chen Hua Instruments, Shanghai, China) in a standard three-electrode system, which

employed a platinum wire as the counter electrode, indium-tin oxide glass (ITO) as the working electrode, and Ag/AgCl (saturated KCl solution) as the reference electrode. 5 mg sample powder was dispersed ultrasonically in 1 mL of ethanol, and 20 μL of the resulting colloidal dispersion (5 mg/mL) was drop-cast onto a piece of ITO slice with a fixed area of 0.5 cm^2 and dried under the infrared lamp to form the sample modified ITO electrode. All the photocurrent measurements were performed at a constant potential of -0.2 V (vs. SCE). Sodium nitrate solution ($NaNO_3$, 0.1 M) was used as the supporting electrolyte for photocurrent measurements. A 500-W Xe arc lamp was utilized as the light source.

2.4 Photocatalytic reactor and photocatalytic activity

The organic dye methylene blue (MB) was used as a model pollutant. It could be known that MB had high photostability and water solubility, making this chemical difficult to be degraded using conventional wastewater treatment methods under visible light. The photocatalytic reaction was performed under a 300W Xe lamp with a 400 nm cutoff filter, and the model of photocatalytic apparatus was shown in **Figure S2a**, and schematic illustration of experimental setup was shown in **Figure S2b**. The photo-catalytic reactor was divided into two parts: one was the water cycle system and the other was the light source system, as shown in **Figure S2b**. The water cycle system controlled the temperature, which avoided interference of thermocatalytic to the light-catalyzed reaction. And the light source system insured the energy of light-catalyzed reaction. Moreover, to ensure that the light source system continued working normally, the water pressure controller was used to protect the light source system.

Typically, 0.025 g of sample was added into 50 mL MB (10 mg/L) in a Pyrex photocatalytic reactor. The air velocity was 2 L/min, and the temperature of reaction was 30°C under constant stirring. Prior to irradiation, the suspensions were magnetically stirred for 30 min in the dark to ensure that the MB could reach the absorption-desorption equilibrium on the photocatalyst surface. At certain time intervals, 3 mL aliquots were sampled and centrifuged to remove the photocatalyst particles. Then the filtrates were analyzed by recording variations of the absorption

band maximum (664 nm) in the UV-vis spectra of MB by using an UV-vis spectrophotometer (UV-2450 Shimadzu).

2.5 Characterization

The obtained CeO_2/g-C_3N_4 composites were characterized by X-ray diffraction (XRD) using Bruker D8 diffractometer with Cu Kα radiation (λ=1.5418 Å) in the range of 2θ=10-80°. The transmission electron microscopy (TEM) images were carried out on a JEOL-JEM-2010 (JEOL, Japan) operated at 200 kV. The Fourier transform infrared spectra (FT-IR) of the samples were recorded using Nicolet Nexus 470 spectrometer. Ultraviolet visible (UV-vis) diffuse reflection spectra were measured using a UV-vis spectrophotometer (Shimadzu UV-2450, Japan) in the range of 200 to 800 nm. $BaSO_4$ was used as reflectance standard material. X-Ray photoelectron spectroscopy (XPS) analysis was performed on an ESCALab MKII X-ray photo-electron spectrometer using Mg Ka radiation.

3. Results and discussion

3.1 TEM and HRTEM analyses

To survey the morphology and microstructure of the CeO_2/g-C_3N_4, it was researched *via* transmission electron microscopy (TEM) (**Figure 1**). In **Figure 1a** and **b**, it was obvious that ultrafine CeO_2 presented cube structure, and the ultrafine CeO_2 nanocubes with size of 3-10 nm were anchored onto the g-C_3N_4. Moreover, the highresolution TEM (HRTEM) image in **Figure 1c** displayed clear (111) lattice fringe with the interplanar spacing of 0.31 nm, implying that the ultrafine CeO_2 nanocubes are enclosed by the (111) planes (JCPDF no. 34-0394), which could be very important for the photocatalytic activity,[24] because an exposed high-activity surface with high crystallinity was very significant to light-catalyzed reaction.[24,29] From the **Figure 1**, it could be known that CeO_2 nanocubes and g-C_3N_4 closely bonded together and they did not separate after a long ultrasonication treatment at room temperature, and formed a heterojunction structure, which was very important to transfer inter-particle electron between component semiconductors. Such cube shapes had rarely been observed for CeO_2 in previous studies.[30]

3.2 XRD and XPS analyses

The crystal structure of CeO_2/g-C_3N_4 composites was further studied by X-ray diffraction (XRD), as shown in **Figure 2**. The diffraction peak of the g-C_3N_4 at ~13.1° correspond to the (100) planes and strong XRD peak of the g-C_3N_4 at ~27.3° are (002) plane,[10] which were interlayer stacking reflections. With increase of the content of CeO_2, the diffraction peaks at ~33.1°, ~47.5° and ~56.3° gradually appeared and intensity increased gradually,[31] and the peaks were assigned to the (200), (220), and (311) planes of CeO_2 crystal (JCPDS no: 34-0394), respectively. However, the diffraction peaks of CeO_2 at ~28.5° assigned to the (111) planes of CeO_2 crystal were not observed from the patterns, which might be because of the relatively low percentage of CeO_2 in the composites, while the diffraction peaks of CeO_2 at ~28.5° might be covered by the strong peak of g-C_3N_4 at 27.3°. Moreover, compared with the g-C_3N_4, in CeO_2/g-C_3N_4 composites, the characteristic interlayer stacking peak of aromatic systems of g-C_3N_4 has changed from ~27.3° to ~27.7°, and this smaller value of diffraction angle might be the attachment of the CeO_2.

To further confirm the composition and the chemical states of the samples, X-ray photoelectron spectroscopy (XPS) measurements were performed and the XPS spectra of C 1s, N 1s for the g-C_3N_4 and C 1s, N 1s, Ce 3d, O 1s for 5% CeO_2/g-C_3N_4 were provided, as shown in **Figure 3**. From **Figure 3a** and **b**, it was found that there was no obvious binding energy shift of C 1s and N 1s for 5% CeO_2/g-C_3N_4 and the g-C_3N_4, suggesting that the chemical states of both carbon and nitrogen in the 5% CeO_2/g-C_3N_4 were the same as in the g-C_3N_4. In **Figure 3a**, the peak located at ~284.6 eV was related to carbon contamination,[32] and was observed in the bulk g-C_3N_4 and 5% CeO_2/g-C_3N_4. The binding energy at ~288.2 eV was assigned to sp^2-bonded carbon (C-N-C) of the g-C_3N_4 in the aromatic ring. In **Figure 3b**, it could be observed that 5% CeO_2/g-C_3N_4 had the same N 1s binding energy of g-C_3N_4 at ~398.7 eV, which could be attributed to sp^2-hybridized nitrogen (C=N-C). Record all above confirmed the presence of sp^2-bonded graphitic carbon nitride in 5% CeO_2/g-C_3N_4. The XPS spectra of O 1s were shown in **Figure 3c**. From **Figure 3c**, two strong peaks at ~529.4 eV and ~531.6 eV for O 1s were obviously observed,

indicating that there were two forms of O species in the sample. The peak at ~529.4 eV was due to the lattice oxygen (O^{2-} in the CeO_2).[33] Whereas the peak at ~531.6 eV was due to the chemisorbed oxygen.[33] Ce 3d XPS spectra of 5% CeO_2/g-C_3N_4 could be assigned to be $3d_{3/2}$ spin-orbit states (labeled **u**) and $3d_{5/2}$ states (labeled **v**), as presented in **Figure 3d**. The bands **v**, **v2**, **v3**, **u**, **u2** and **u3** were attributed to Ce^{4+}, whereas **v1** and **u1** are due to Ce^{3+}.[33-35] From **Figure 3d**, it could be found that the coexistence of Ce^{3+}/Ce^{4+} oxidation states existed on the surface of the catalysts, which indicated that the catalyst surfaces might be not fully oxidized. According to the previous reports,[22,35] these might lead to the conclusion that some oxygen vacancies might be produced.[22,35] Records above might be very important to the performance of the photocatalyst, and the further research is still needed.

3.3 FT-IR, DRS and Photocurrent-time analyses

To make the structure of CeO_2/g-C_3N_4 clearly, the samples were analyzed by FT-IR spectra, as shown in **Figure 4a**. The FT-IR spectrum of various CeO_2/g-C_3N_4 was similar to g-C_3N_4, indicating that g-C_3N_4 in CeO_2/g-C_3N_4 kept the same chemical structure as g-C_3N_4. The broad peaks between 3600 and 3000 cm^{-1} were caused by the N-H stretches, indicating that there could be dangling hydrogens in the C-N layers of the g-C_3N_4. The peaks at ~1242, 1322, 1412, 1563, and 1634 cm^{-1} were typical stretching vibration modes of C=N and C-N heterocycles.[9,32,36] The peak at 807 cm^{-1} was the characteristic breathing mode of s-triazine ring system.[32,36] And all characteristic vibrational peaks related to g-C_3N_4 could also be found in various CeO_2/g-C_3N_4, indicating that the structural integrity of g-C_3N_4 remained intact after the hydrothermal reaction.

To identify the photoelectric property and electronic structure of various CeO_2/g-C_3N_4, UV-vis diffuse reflectance spectroscopy (DRS) was used, as shown in **Figure 4b**. And it could be known that the UV-visible absorption spectrum of various CeO_2/g-C_3N_4 displayed a slight blue shift in comparison with the g-C_3N_4. The blue shift could be caused by the famous quantum confinement effect with the conduction and valence bands shifing in opposite directions.[37-39] From **Figure 4c**, it could be known that the bandgaps of the g-C_3N_4, 2.5% CeO_2/g-C_3N_4, 5% CeO_2/g-C_3N_4 and

10% CeO_2/g-C_3N_4 were about 2.65, 2.83, 2.81 and 2.79 eV, respectively.

To make sure 5% CeO_2/g-C_3N_4 was an excellent photocatalyst, its electronic structure, photogenerated charge separation and electron transfer performance were investigated by the photocurrent-time analyse, as shown in **Figure 4d**. Under visible light irradiation, compared with g-C_3N_4 and the other mass samples, 5% CeO_2/g-C_3N_4 showed the best photocurrent responses, which was about twice higher than g-C_3N_4. What's more, the photocurrents of 2.5% and 10% CeO_2/g-C_3N_4 were less than 5% CeO_2/g-C_3N_4 and they were close. Obviously, an appropriate CeO_2 ratio was very significant for increasing the photocurrent responses. The increased photocurrents of 2.5%, 5% and 10% CeO_2/g-C_3N_4 were due to the improved photoabsorption and photoresponsivity. Obviously, 5% CeO_2/g-C_3N_4 had less recombination and a more efficient separation of photogenerated electron and hole pairs, compared with g-C_3N_4 and the other mass content. Thus, 5% CeO_2/g-C_3N_4 could have the fascinating photocatalytic performance.

3.4 Nitrogen adsorption analysis

The Brunauer-Emmett-Teller (BET) specific surface area of all samples were carried out. From **Figure S3**, it could be known that the specific surface area of g-C_3N_4, 2.5%, 5% and 10% CeO_2/g-C_3N_4 were ~3.3, 68.4, 78.8 and 96.3 m^2/g, respectively. The surface area improved a lot, as the introduction of CeO_2 to g-C_3N_4. And BET of the composites were increased with the contents of CeO_2 increased from 2.5% to 10%, which could be caused by the interaction of CeO_2 and g-C_3N_4. It could be known that the large surface area was beneficial to the photocatalytic activity increase, due to more adsorption sites and photocatalytic reaction centers. Thus, CeO_2/g-C_3N_4 composites could have excellent photocatalytic performance.

3.5 Photocatalytic activity test and and kinetics

The photocatalytic activity of the samples for the degradation of MB was evaluated under visible light irradiation, as shown in **Figure 5a**. The photocatalytic activity of the pure g-C_3N_4 was the lowest and the photocatalytic degradation efficiency was only ~56% after 3.5 h of visible light irradiation. Meanwhile, ~86.07%, ~89.16% and ~98.59% of MB were degraded using 10%

CeO_2/g-C_3N_4, 2.5% CeO_2/g-C_3N_4 and 5% CeO_2/g-C_3N_4, respectively. Obviously, 5% CeO_2/g-C_3N_4 had the optimal photocatalytic activity for MB decomposition, and an appropriate CeO_2 ratio in CeO_2/g-C_3N_4 nanocomposites could significantly improve the resulting photocatalytic activity. Moreover, from data above, it could be known that the photocatalytic degradation efficiency of the CeO_2/g-C_3N_4 composites was obviously and extensively improved, compared with the g-C_3N_4, and the optimal percentage of CeO_2/g-C_3N_4 was 5%. Moreover, the result in **Figure 5c** indicated that after 4 cycles, the photocatalytic activity of the 5% CeO_2/g-C_3N_4 only reduced a little, which could due to the loss of the photocatalyst during the experiments. Therefore, for industrial application, 5% CeO_2/g-C_3N_4 should be considered. In addition, XRD (**Figure 6a**) and FT-IR (**Figure 6b**) analysises of 5% CeO_2/g-C_3N_4 before and after the photocatalytic reactions was carried out. Obviously, both XRD and FT-IR spectra of 5% CeO_2/g-C_3N_4 before and after the photocatalytic reactions were similar. That is to say, the crystal structures and chemical structures of 5% CeO_2/g-C_3N_4 didn't change after photocatalytic cycle, which obviously suggested that 5% CeO_2/g-C_3N_4 were stable during the photodegradation process.

The large BET could offer more adsorption sites and photocatalytic reaction centers. But the specific surface area was not a crucial factor for improving photocatalytic activity in CeO_2/g-C_3N_4 system. When the weight content of CeO_2 was increasing to 10%, the degradation rate of MB decreased, and the reason should be explained as follows: firstly, when the contents of CeO_2 increased to 10%, although the sample's BET was the largest, a large amount of CeO_2 wrapped on the surface of g-C_3N_4, which hindered that g-C_3N_4 absorbed light. Secondly, a dense mass of CeO_2 cubes on the surface of g-C_3N_4 were not conducive to form heterojunction structure, yet could lead to the self-destruction of heterojunction structure.[9] Thirdly, a large amount of CeO_2 cubes wrapping on the surface of g-C_3N_4 were harmful to the separation of electrons and holes, which leads to the reduction of the active sites in the CeO_2/g-C_3N_4 composites. All in all, the degradation rate of MB decreased when the weight content of CeO_2 was increasing to 10%. The optimal percentage of CeO_2/g-C_3N_4 was 5%.

The variations of UV-vis absorption spectras of MB degradation using g-C_3N_4 and CeO_2/g-C_3N_4 composites were shown in **Figure 7a-d**. It was obvious that after visible light illumination, with 5% CeO_2/g-C_3N_4 composites, the color of MB solution changed from blue to colourless during the reaction, as shown in **Figure 7c** and in the inset of **Figure 7c**. The peak intensity of the UV-vis absorption related to MB decreased sharply, and the main absorption band at 664 nm almost completely disappeared after 3.5 h, which indicated the chromophoric structure of the MB dye was decomposed. Improved photocatalytic activity could be ascribed to the synergistic effects of the effective combination of ultrafine CeO_2 cubes on g-C_3N_4, high crystallinity of the sample and the facile optical properties.

To understand the process of the light-catalyzed reaction, kinetics was used to analyze. It could be known that the kinetics of heterogeneous catalysis of a liquid-solid system has frequently been described using Langmuir-Hinshelwood (L-H) model,[9] which was **Equation 1**.

$$r = -\frac{dC}{dt} = \frac{k_r KC}{1 + KC + K_s C_s} (1) \qquad r = -\frac{dC}{dt} = \frac{k_r KC}{1 + KC} (2)$$

In **Equation 1**, k_r is the reaction rate constant, C is the concentration of the reactant, t is the reaction time, K_s is the adsorption coefficient of the solvent, K is the adsorption coefficient of the reactant and C_s is the concentration of the solvent. When the reactant is more strongly adsorbed than solvent, **Equation 1** could be simplified to **Equation 2**. When the initial concentration of reactant is very low ($KC \ll 1$), **Equation 2** can be further simplified to **Equation 3**, where k_{app} represents the apparent reaction rate constant.

$$r = -\frac{dC}{dt} = k_r KC = k_{app} C (3)$$

According to the previous work,[9,40,41] it can be known that the photocatalytic reaction of MB can be described by the simplified L-H model. And **Equation 3** can be written **Equation 4:**

$$r = k_r KC_{MB} = k_{app} C_{MB} (4)$$

Moreover, the linear relationship of $\ln(C_0/C)$ versus time is shown in **Figure 5b** and the kinetic constant (k) and regression coefficient (R^2) were calculated and given in *Table 1*. The results indicated that for all investigated photocatalysts, the photocatalytic degradation of MB followed first-order reaction dynamics under the experimental conditions. From **Figure 5b**, 5% CeO_2/g-C_3N_4 exhibited high apparent rate of 1.2686 h^{-1}, which was 7.8 times as high as than that of g-C_3N_4 (0.1621 h^{-1}), and the k for MB degradation with the 2.5% and 10% CeO_2/g-C_3N_4 composites were estimated to be 0.5687 and 0.6226 h^{-1}, respectively.

3.6 Photoelectrochemical selective sensing of Cu^{2+}

On account of increasing photocurrent intensity of 5% CeO_2/g-C_3N_4, excellent charge-carrier-transfer behavior and charge separation, 5% CeO_2/g-C_3N_4 was an ideal candidate material for photoelectrochemical application. On the other hand, owing to the fact that the photocurrent intensity of the g-C_3N_4 was low-grade, as shown in **Figure 4d**, from the comparison of 5% CeO_2/g-C_3N_4 composites and g-C_3N_4 for the detection of trace amounts of Cu^{2+}, the photocurrent intensity of g-C_3N_4 was not sensitive enough, which was discussed in our previous work.[32,42,43] Therefore, in g-C_3N_4-supported CeO_2 cubes, because of the more sensitive photoelectrochemical performance of 5% CeO_2/g-C_3N_4, it had been evaluated by the sensing of trace amounts of Cu^{2+} which was an essential element for living organisms but toxic at high concentrations.[32,44] The rule of Cu^{2+} concentration on the photocurrent at the ITO/5% CeO_2/g-C_3N_4 electrode was found to be concentration-dependent in **Figure 8a**. The photocurrent of 5% CeO_2/g-C_3N_4 gradually increased when the concentration of Cu^{2+} increased. What's more, a good linear relationship (R^2 = 0.9956) could be seen between the value of the photocurrent increasing. And the linear equation was y =0.3056x + 5.8184, as shown in **Figure 8b**. The photocurrent intensities of ITO/5% CeO_2/g-C_3N_4 electrode in the presence and absence of Cu^{2+} and the concentration of Cu^{2+} over the range from 0 to 10 μM are very significant for the detection of trace amounts of Cu^{2+}.

The mechanism of photoelectrochemical selective sensing of trace amounts of Cu^{2+} was discussed in detail, as shown in **Figure 9**. When 5% CeO_2/g-C_3N_4 was

irradiated with visible light, it absorbed photons, meanwhile it excited electron and hole pairs. Based on the band gap theory,[32,42,45] the band gap of CeO_2 was 2.92 eV, which was higher than that of g-C_3N_4 (2.65 eV). The excited electrons in the conduction band of g-C_3N_4 could be easily transferred to surface of the CeO_2, and then transferred to the ITO electrode and generated the photocurrent because the energy level of the conduction band of ITO was low.[32,42,43] And the generated holes could move to the surface of g-C_3N_4,[9] which promoted the effective separation of photoexcited electron-hole pairs and decreased the probability of electron and hole recombination.[9,32,42,43] Then photoexcited electrons moved to the ITO and then to the Pt electrode, so it could formed a closed circuit. In the presence of Cu^{2+}, Cu^{2+} could be seen as the electron acceptor. The excited and transferred electrons could be accepted by Cu^{2+} to form metal Cu, and then metal Cu deposited on the Pt electrode.[43] This phenomenon can be observed when the duration of light was extended:[43] There were tiny yellow metal Cu particles on the surface of Pt electrode as Cu^{2+} could capture the electrons and continuously form metal Cu, and the details were in previous work.[32,42,43] According to previous reports,[42,43] it could be known that the selection determination of Cu^{2+} could mainly come from g-C_3N_4 in the CeO_2/g-C_3N_4 composite. Although g-C_3N_4 had detection signal for selection determination for Cu^{2+}, g-C_3N_4's photocurrent intensity was not high enough. Thus, the sensitivity of Cu^{2+} is weak. Nevertheless, 5% CeO_2/g-C_3N_4 had the better photocurrent, which overcame g-C_3N_4's defects of the weak photocurrent well. The function of the appropriate CeO_2 in the composite could be to transfer electrons, which resulted in the less recombination and a more efficient separation of photogenerated electron and hole pairs. Thus, the selection determination of Cu^{2+} could mainly come from g-C_3N_4, the introduction of CeO_2 improved the sensitivity of the determination for Cu^{2+}. Finally, the synergistic effect of CeO_2 and g-C_3N_4 led to the selective and sensitive detection of trace amounts Cu^{2+}.

Compared with traditional methods of the detection of trace amounts of Cu^{2+}, such as flame atomic absorption method, the photoeletrochemical method is especially suited to selectively sense of the trace concentration of Cu^{2+}, as well as

sensitive, simple, timesaving and economic which due to this method avoids the preconcentration process and relatively expensive apparatus required for the fluorescence method, flame atomic absorption method.

To assess the selectivity of the 5% CeO_2/g-C_3N_4 as well as to trace amounts of Cu^{2+}, the effect of different metal ions (Ag^{+}, Co^{2+}, Cr^{3+}, Fe^{3+}, Cu^{2+}, Hg^{2+}, Mn^{2+}, Ni^{2+}, Pb^{2+} and Zn^{2+}) with the concentration of 4.0 μM on the photocurrent intensities were investigated, as shown in **Figure 8c**. It could be effectively observed that the ITO/5% CeO_2/g-C_3N_4 electrode was much more sensitive to Cu^{2+} than to the other metal ions. Owing to the highly sensitive and selective increased effect of Cu^{2+} on the photocurrent intensity of ITO/5% CeO_2/g-C_3N_4 electrode, a highly selective and sensitive sensor for the detection of Cu^{2+} was further developed in metal oxide composites.

4. Conclusions

Finally, the CeO_2/g-C_3N_4 composites were prepared successfully by a simple and facile hydrothermal method. Thereinto, CeO_2 with 111 planes was in the shape of the cube (from ~3 to 10 nm). After the introduction of CeO_2, the photocatalytic activities of g-C_3N_4 on MB degradation under visible light irradiation increased dramatically. The results indicated that 5% CeO_2/g-C_3N_4 exhibited the optimal photocatalytic performance. The further studies confirmed that 5% CeO_2/g-C_3N_4 could be used as for the detection of trace amounts Cu^{2+} in water environment. In addition, the excellent photocatalytic reactor had also been exploited successfully, which could promote the further development of photocatalysis technology. In conclusion, this report could be useful for preparation of particles, especially with a view to filtrating photocatalyst, promoting the material properties and expanding the practical application of the photocatalysis technology.

Acknowledgements

The authors genuinely appreciate the financial support of this work from the National Nature Science Foundation of China (21177050, 21476097, 21407065, 21406094), Natural Science Foundation of Jiangsu Province (BK20131207, BK20140533), Postdoctoral Foundation of China (2014M551520).

Notes and References

1. X. B. Chen and S. S. Mao, *Chem. Rev.*, 2007, 107, 2891.
2. S. W. Liu, J. G. Yu and M. Jaroniec, *J. Am. Chem. Soc.*, 2010, 132, 11914.
3. W. Li, J. P. Yang, Z. X. Wu, J. X. Wang, B. Li, S. S. Feng, Y. H. Deng, F. Zhang and D. Y. Zhao, *J. Am. Chem. Soc.*, 2012, 134, 11864.
4. W. Li, F. Wang, S. S. Feng, J. X. Wang, Z. K Sun, B. Li, Y. H. Li, J. P. Yang, A. A. Elzatahry, Y. Y Xia and D. Y. Zhao, *J. Am. Chem. Soc.*, 2013, 135, 18300.
5. R. S. Manea, S. J. Roha, O. S. Joob, C. D. Lokhande and S. H. Han, *Electrochim. Acta*, 2005, 50, 2453.
6. X. J. Feng, K. Zhu, A. J. Frank, C. A. Grimes and T. E. Mallouk, *Angew. Chem. Int. Ed.*, 2012, 51, 2727.
7. Y. Wang, X. C. Wang and M. Antonietti, *Angew. Chem. Int. Ed.*, 2012, 51, 68.
8. X. C. Wang, K. Maeda, A. Thomas, K. Takanabe, G. Xin, J. M. Carlsson, K. Domen and M. Antonietti, *Nat. Mater.*, 2009, 8, 76.
9. H. Xu, J. Yan, Y. G. Xu, Y. H. Song, H. M. Li, J. X. Xia, C. J. Huang and H. L. Wan, *Appl. Catal., B*, 2013, 129, 182.
10. X. D. Zhang, X. Xie, H. Wang, J. J. Zhang, B. C. Pan and Y. Xie, *J. Am. Chem. Soc.*, 2013,135, 18.
11. X. C. Wang, S. Blechert and M. Antonietti, *ACS Catal.*, 2012, 2, 1596.
12. S. Chu, Y. Wang, Y. Guo, J. Y. Feng, C. C. Wang, W. J. Luo, X. X. Fan and Z. G. Zou, *ACS Catal.*, 2013, 3, 912.
13. X. J. Bai, R. L. Zong, C. X. Li, D. Liu, Y. F. Liu and Y. F. Zhu, *Appl. Catal., B*, 2014, 147, 82.
14. D. M. Chen, K. W. Wang, D. G. Xiang, R. L. Zong, W. Q. Yao and Y. F. Zhu, *Appl. Catal., B*, 2014, 147, 554.
15. S. F. Chen, Y. F. Hu, S. G. Meng and X. L. Fu, *Appl. Catal., B*, 2014, 150, 564.
16. X. J. Bai, L. Wang, Y. J. Wang, W. Q. Yao and Y. F. Zhu, *Appl. Catal., B*, 2014, 152, 262.
17. J. Chen, S. H. Shen, P. H. Guo, M. Wang, P. Wu, X. X. Wang and L. J. Guo, *Appl.*

Catal., B, 2014, 152, 335.

18. X. F. Chen, J. S. Zhang, X. Z. Fu, M. Antonietti and X. C. Wang, *J. Am. Chem. Soc.*, 2009, 131, 11658.
19. X. X. Zou, J. Su, R. Silva, A. Goswami, B. R. Sathe and T. Asefa, *Chem. Commun.*, 2013, 49, 7522.
20. J. W. Lee, H. J. Jeon, H. J. Shin and J. K. Kang, *Chem. Commun.*, 2012, 48, 422.
21. C. G. Silva and J. L. Faria, *ChemSusChem*, 2010, 3, 609.
22. H. J. Yan and H. X. Yang, *J. Alloys Compd.*, 2011, 509, 26.
23. S. C. Hu, F. Zhou, L. Z. Wang and J. L. Zhang, *Catal. Commun.*, 2011, 12, 794.
24. L. H. Jiang, M. G. Yao, B. Liu, Q. J. Li, R. Liu, H. Lv, S. C. Lu, C. Gong, B. Zou, T. Cui, B. B. Liu, G. Z. Hu and T. Wagberg, *J. Phys. Chem. C*, 2012, 116, 11741.
25. A. Trovarelli, *Catal. Rev. Sci. Eng.*, 1996, 38, 439.
26. Z. L. Wang, G. R. Li, Y. N. Ou, Z. P. Feng, D. L. Qu and Y. X. Tong, *J. Phys. Chem. C*, 2011, 115, 351.
27. A. Corma, P. Atienzar, H. Garcia and J. Y. Chane-Ching, *Nat. Mater.*, 2004, 3, 394.
28. Y. F. Yu, Y. M. Zhu and M. Meng, *Dalton Trans.*, 2013, 42, 12087.
29. N. Skorodumova, M. Baudin and K. Hermansson, *Phys. Rev. B*, 2004, 69, 075401.
30. Y. Yamada, C. K. Tsung, W. Huang, Z. Y. Huo, S. E. Habas, T. Soejima, C. E. Aliaga, G. A. Somorjai and P. D. Yang, *Nature Chem.*, 2011, 3, 372.
31. W. D. Cai, F. Chen, X. X. Shen, L. J. Chen and J. L. Zhang, *Appl. Catal., B*, 2010, 101, 160.
32. H. Xu, J. Yan, X. J. She, L. Xu, J. X. Xia, Y. G. Xu, Y. H. Song, L. Y. Huang and H. M. Li, *Nanoscale*, 2014, 6, 1406.
33. T. Hasegawa, S. M. F. Shahed, Y. Sainoo, A. Beniya, N. Isomura, Y. Watanabe and T. Komeda, *Chin. J. Chem. Phys.*, 2014, 140, 044711.
34. C. X. Liu, L. Chen, J. H Li, L. Ma, H. Arandiyan, Y. Du, J. Y. Xu and J. M. Hao, *Environ. Sci. Technol.*, 2012, 46, 6182.
35. R. Zhang, Q. Zhong, W. Zhao, L. M. Yu and H. X. Qu, *Appl. Surf. Sci.*, 2014, 289,

237.

36. S. B. Yang, Y. J. Gong, J. S. Zhang, L. Zhan, L. L. Ma, Z. Y. Fang, R. Vajtai, X. C. Wang and P. M. Ajayan, *Adv. Mater.*, 2013, 25, 2452.
37. J. H. Sun, J. S. Zhang, M. W. Zhang, M. Antonietti, X. Z. Fu and X. C. Wang, *Nat. Commun.*, 2012, 3, 1139.
38. X. C. Wang, K. Maeda, X. F. Chen, K. Takanabe, K. Domen, Y. D. Hou, X. Z. Fu and M. Antonietti, *J. Am. Chem. Soc.*, 2009, 131, 1680.
39. A. L. Linsebigler, G. Q. Lu and J. T. Yates, *Chem. Rev.*, 1995, 95, 735.
40. H. Xu, C. Wang, Y. H. Song, J. X. Zhu, Y. G. Xu, J. Yan, Y. X. Song, H. M. Li, *Chem. Eng. J.*, 2014, 241, 35.
41. J. J Chen, J. X. Zhu, Z. L. Da, H. Xu, J. Yan, H. Y. Ji, H. M. Shu, H. M. Li, *Appl. Surf. Sci.*, 2014, 313, 1.
42. X. J. She, H. Xu, Y. G. Xu, J. Yan, J. X. Xia, L. Xu, Y. H. Song, Y. Jiang, Q. Zhang and H. M. Li, *J. Mater. Chem. A*, 2014, 2, 2563.
43. L. Xu, J. X. Xia, H. Xu, J. Qian, J. Yan, L. G. Wang, K. Wang and H. M. Li, *Analyst.*, 2013,138, 6721.
44. Q. M. Shen, X. M. Zhao, S. W. Zhou, W. H. Hou and J. J. Zhu, *J. Phys. Chem. C*, 2011, 115, 17958.
45. P. Niu, L. L. Zhang, G. Liu and H. M. Cheng, *Adv. Funct. Mater.*, 2012, 22, 4763.